Curvature sculptured growth of plasmonic nanostructures by supramolecular recognition

Sui Yang,[1] Yuan Wang,[1] and Xiang Zhang[1,2,*]

[1]*Nano-scale Science and Engineering Center (NSEC), 3112 Etcheverry Hall, University of California, Berkeley, California 94720, USA*
[2]*Faculties of Sciences and Engineering, University of Hong Kong, Hong Kong, China*

Nanoscale curvature is an important and powerful tool in understanding and tailoring chemical/surface functionalities of nanostructures that dictate a host of important applications from biochemical recognitions, catalysis to spectroscopy. However, it is a critical challenge in materials chemistry to rationally shape the local nanoscale curvatures of colloidal nanoparticles during the growth owing to the constraints of their flat facets. Here we demonstrate a synthetic mechanism that could cooperatively mediate local nanoparticle surface curvature patchiness and shape symmetries during one-step colloidal growth. The idea is to tailor host-guest supramolecular recognition using fluorocarbon and hydrocarbon molecules that regulate interfacial energy during the nanoparticle growth. Such delicate regulation enables a degree of freedom in control over the local nanoparticle curvatures during the growth, resulting in intriguing plasmonic properties. More interestingly, a morphological shape transformation was induced by such curvature changes from anisotropic nanorods to isotropic nanospheres. This unique approach of the spontaneous curvature/structural transformation of plasmonic nanoparticles exploits the mutual interplay between competing supramolecules and colloidal growth. It may ultimately allow for accurate controlling nanoscale objects with varied degree of complexity that could open the door to a myriad of surface chemical, optical, and biomedical applications.

I. INTRODUCTION

While size and shape of nanostructured materials significantly affect their physicochemical properties, nanocurvature, a differential geometric property at the nanoscale, plays a distinct and central role in determining surface chemical functionality of the final nano-objects [1]. As evidenced, nanoscopic surface curvatures significantly modulate nanostructure-biomolecule (nanobio) interactions through the changes of confirmations and functionalities of biomolecules in different local surface environments [2,3]. In another aspect, controlling the local curvatures of nanostructures could lead to distinct surface chemical potentials that expose catalytically active sites making high effective catalysts [4].

It has been shown how local curvatures can affect the immobilization and dissociation behavior of surface-bound ligands [5–8]. Specifically, curvature alterations can regulate the surface chemical states of nanoparticle known as Gibbs-Thomson effect [9]. For example, pKa of coated ligands on curved spherical nanoparticles is demonstrated to have more than two pH units as compared to that of the normal pKa in water [8]. Such an efficient surface control provides a fundamental way to directly engineer the local electrostatic potential "electrostatic patchiness" on nanoparticles [10]. However, the surface curvature usually cannot be easily controlled during the synthesis and most curvature manipulations are restricted to simple spherical nanoparticles with its inverse relation to the particle radius. Due to smooth crystal facets and nontrivial size-curvature relation of anisotropic/arbitrary-shaped nanoparticles, it remains critical challenges to synthesize and manipulate such local geometric factor and chemical patchiness at the nanoscale.

Here we report a synthetic chemistry approach that could cooperatively synthesize and sculpt local nanoparticle surface curvatures and shape symmetries during one-step growth. The key idea is to use supramolecular host-guest recognitions that regulate the local interfacial energy between supramolecular template and inorganic precursors during the growth, sculpturing local surface curvatures of nanoparticles. Manipulation of such local curvature patchiness and geometric transformation generates desired and high-quality plasmonic properties that could open up a rich variety of important applications ranging from biochemical reactions, optical and sensing devices, to heterogeneous catalysis [11–14].

As a demonstration model, we targeted colloidal gold nanorods (AuNRs) system, which offers localized surface plasmon resonance over a broad range of spectra and leads to vast technologies and applications including imaging, solar cells, metamaterials, and spectroscopies [15–18]. Utilizing well-developed seed-mediated growth method, all previous wet chemical approaches to grow AuNRs are limited to the control of size and aspect ratios (AR: length/width) [19–24]. To achieve the local control of surface curvatures, we developed a supramolecular templating scheme by hydrocarbon (host molecule) -fluorocarbon (guest molecule) recognition (Fig. 1).

II. METHOD

Specifically, perfluoro-octanoic acid (PFOA), a negatively charged fluorocarbon molecule is introduced, which is strongly coupled to positively charged cetyltrimethylammonium bromide (CTAB) molecules in solution [25,26]. The
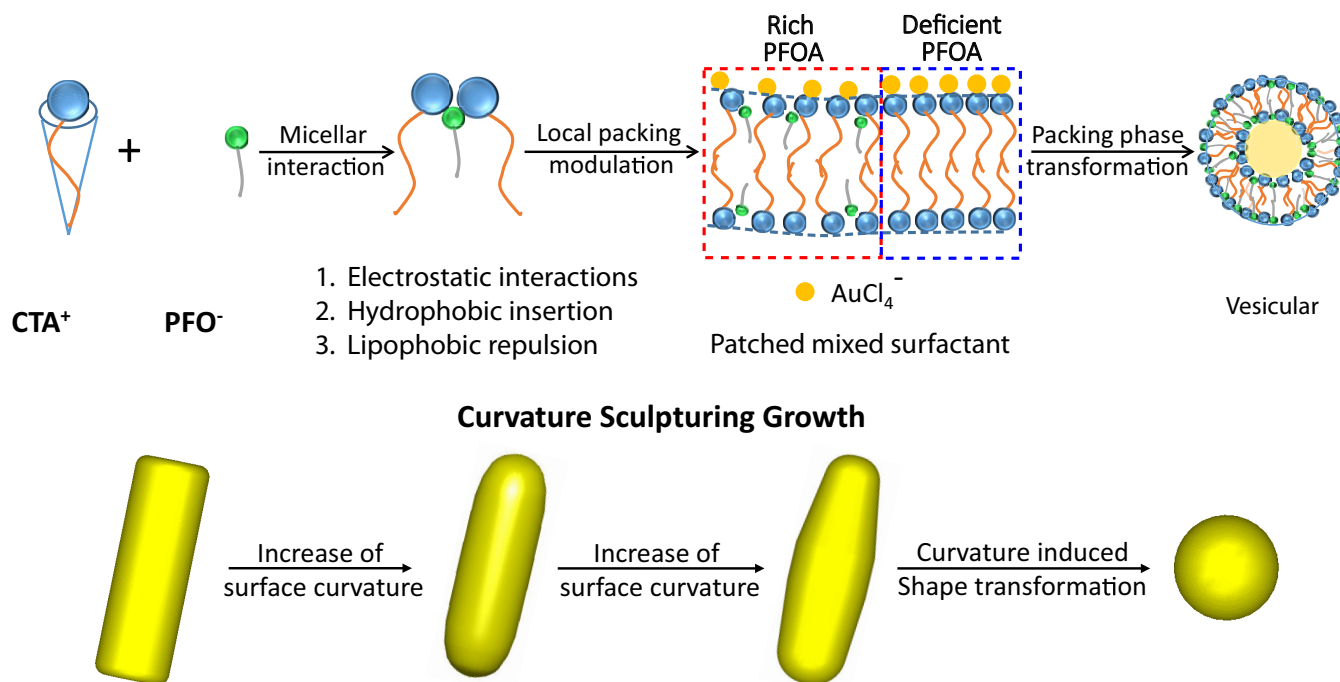
*xiang@berkeley.edu

FIG. 1. Schematic illustration of surface curvature sculpturing growth of colloidal plasmonic gold nanoparticles. The uniqueness of the approach is to introduce fluorocarbon molecule that possesses both hydrophobic and lipophobic properties. The compromised host (hydrocarbon CTA$^+$)-guest (fluorocarbon PFO$^-$) recognitions are through (1) electrostatic attraction, (2) hydrophobic insertion, and (3) lipophobic repulsion. Such synergistic supramolecular interactions thus generate microphased inhomogeneity of coupled micelle, structural directing template and modulates its interfacial energy. Due to the direct proportional relationship between surface energy and surface curvature, these unique compromised interactions simultaneously regulate surface curvature patchiness and growth of gold nanoparticles. More specifically, PFOA/CTAB micelle regulates the local packing parameter and charge density that binds to gold precursor ion, which governs the growth of curved gold nanoparticle and eventually leads to morphological transformation.

host-guest recognition could lead to synergism effect of intermolecular coupling, and thus regulate the growth in two aspects: (1) transforming shape and phase of mixed micellar structures that alter the adsorption density and surface energy of preferentially binding surfactants on gold surface [27]; (2) more importantly, the uniqueness of fluorocarbon chain in PFOA can cause both hydrophobic (attractive) and lipophobic (repulsive) interactions with hydrocarbon chain in CTAB due to high electronegativity of fluorine atom. Such competing interfacial fluorocarbon-hydrocarbon interaction leads to inhomogeneous microphased compartments distributed over the binding micelles [28–30]. It therefore induces microcharged surface inhomogeneity that interacts differently with gold precursor species and governs the formation of local surface curvatures along the resulting nanoparticle. The curvature sculptured synthesis utilizing hydrocarbon-fluorocarbon supramolecular coupling is thus fundamentally in contrast to traditional seed-mediated methods [19,20] or growth by either using additives or binary surfactants [22,23,31].

We initiate the growth by preparing viscoelastic micellar solution of PFOA and CTAB to control synergistic micellization, with their molecular ratio designed by R. Subsequently, as-prepared complex micellar solution (denoted by R) was gently mixed with HAuCl$_4 \cdot$ 3H$_2$O (1.8 mg) and slowly stirred for 30 min, allowing gold precursor diffused into micelle sites. The growth was induced by adding reducing agent ascorbic acid and seed solution which is prepared as similar to seed-

mediated method (details in Supplemental Material, Sec. 1 [32]). The final product was centrifuged and collected without further size and/or shape purification.

III. RESULTS AND DISCUSSION

To illustrate the unique ability to control surface curvatures, transmission electron microscopy (TEM) images of AuNRs are shown at equivalent aspect ratios for facile comparison with selectively synthesized at $R = 0$, 0.11, and 0.125 [Figs. 2(a)–2(c)]. Even though all three samples have similar sizes and present a similar averaged aspect ratio ∼2.9 (Supplemental Material [32], Fig. S1), they display completely different nanoscopic local surface curvatures (indicated as k). Without adding PFOA ($R = 0$), AuNRs show relative flat edges and corner with small k [Fig. 2(d)]. However, when the synergistic micellization is formed by fluorocarbon and hydrocarbon coupled supramolecules ($R = 0.11$ and 0.125), such geometric factor k changes dramatically as more rounded head tips and curved edges are observed. Clear surface patchiness with distinct curvature values (both positive and negative k) have been observed in the surface profile of each representative AuNRs [Fig. 2(d) and Supplemental Material, Sec 3]. Increasing R leads to more curved surface (large k) and eventually displays a "bullet"-like shape with quite sharp tips. The patchy curvatures and $\pm k$ become much wider distributed as reflected by their color values across their boundaries with
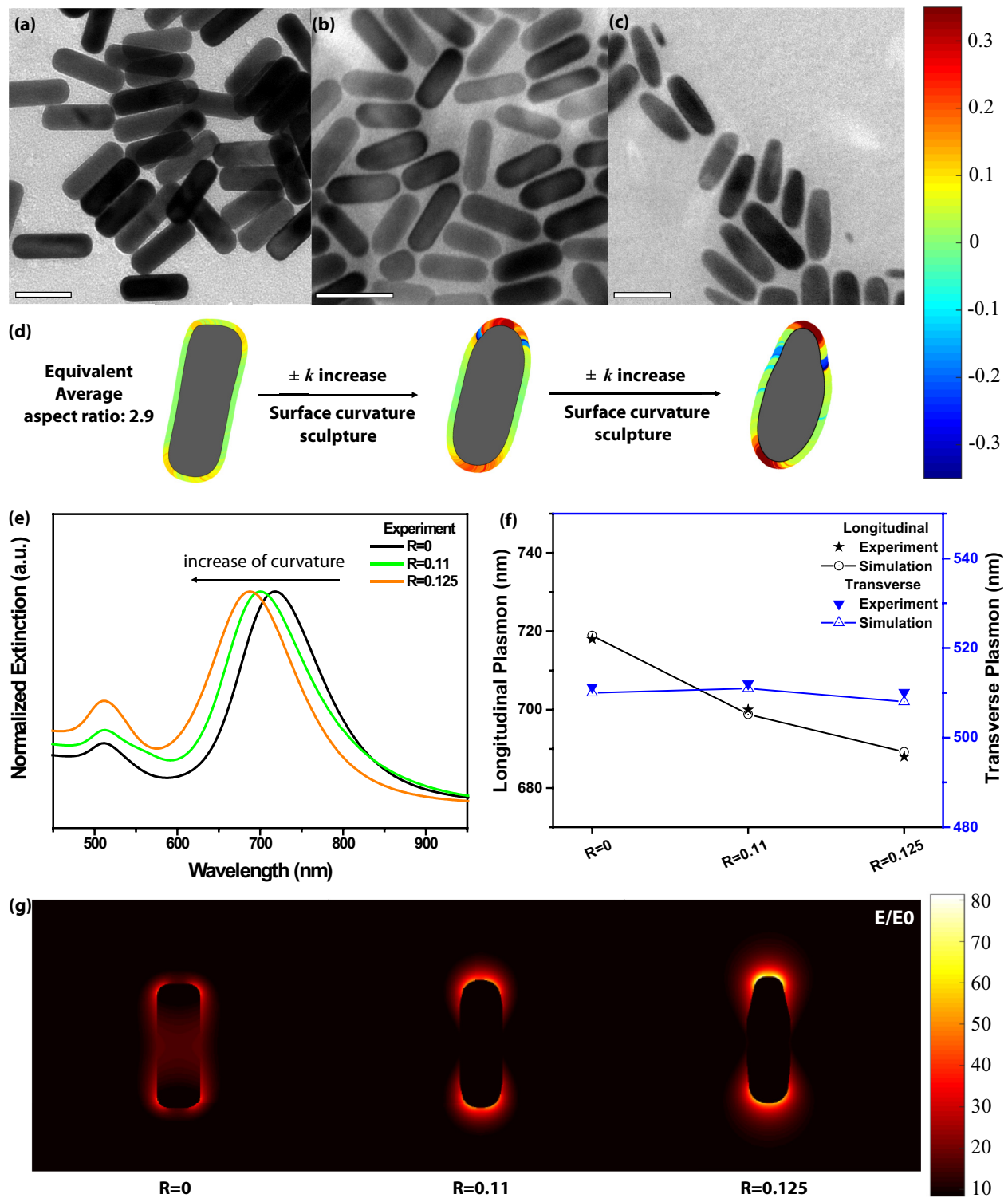
FIG. 2. Surface curvature sculptured growth of colloidal gold nanorods and related properties. (a)–(c) TEM images of gold nanorods at the equivalent aspect ratio of 2.9 but with distinct surface curvatures at synthetic parameters (a) $R = 0$; (b) $R = 0.11$, and (c) $R = 0.125$. Scale bar is 50 nm. (d) The quantitative analysis of local surface curvature (k) of synthesized gold nanorods represented by different curvatures as values indicated in colormap as unit of nm^{-1}. (e) Plasmonic responses of curvature sculptured synthesized nanorods (extinction spectra normalized by the geometry cross section). Different colored curves indicate different R values. (f) Comparison between experimental and simulated data at resonance maximum for both longitudinal and transverse plasmon. Appreciable blueshift of longitudinal resonances was shown due to the surface curvature change, while transverse plasmon peak almost remains as for the quasistatic limit. (g) Calculated plasmonic energy confinement with normalized electric-field enhancement (E/E_0) at resonant maximum for gold nanorods (distinct curvatures but same aspect ratio). Color bar indicates the relative electric-field enhancement values. The highly curved surface of nanorod leads to much stronger confinement of plasmon energy at designated high-k location.
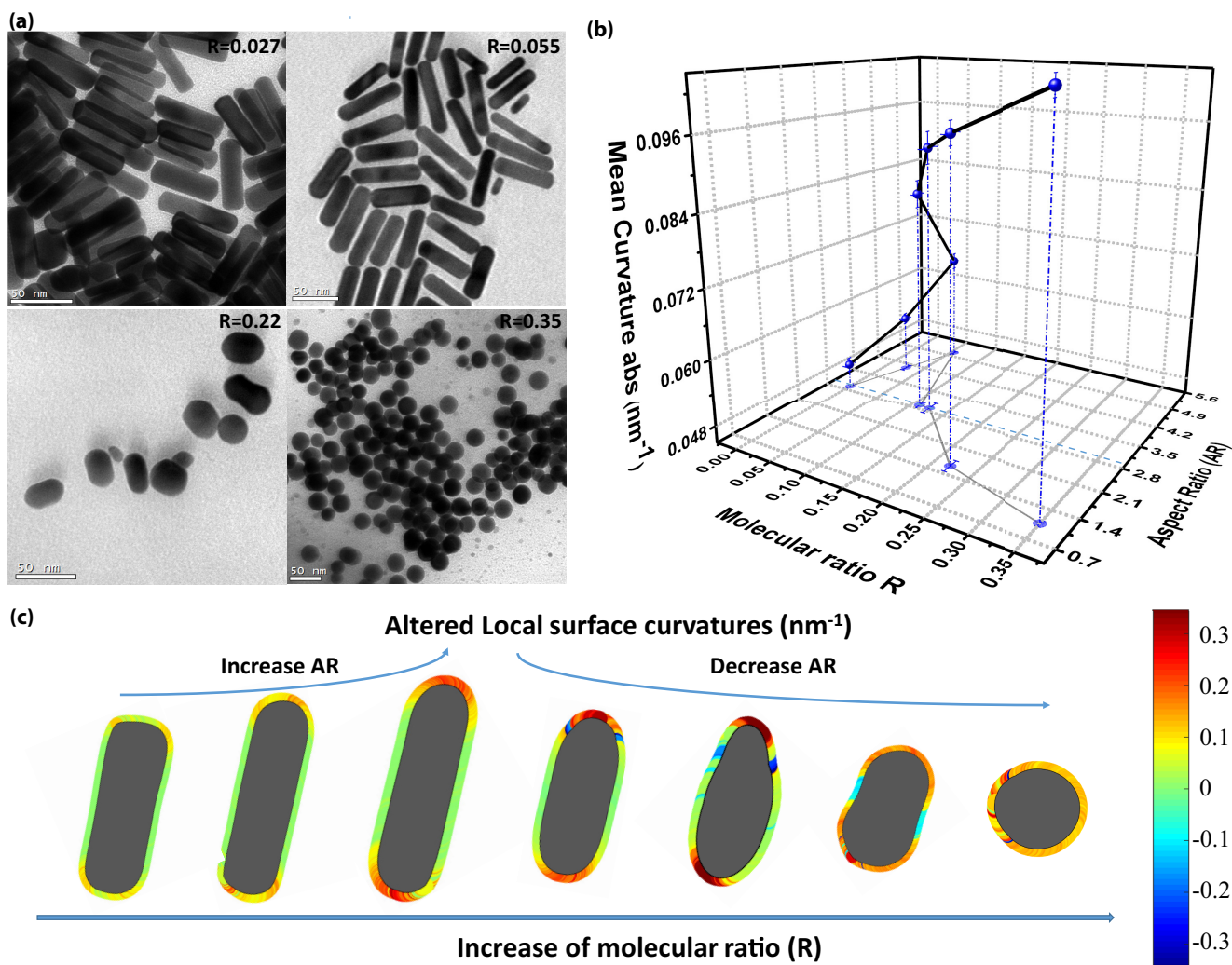
FIG. 3. Synergistic surface curvature and shape anisotropicity control. (a) TEM images of gold nanostructure transformation by systematically increasing PFO^{-} (R) in the synthesis. As increasing R up to 0.055, the head tips of AuNRs become rounded and the shape elongated. However, the anisotropy of gold changes inversely with shortened aspect ratio and even more rounded edges as further increasing R and finally leading to nanospheres ($R = 0.35$). (b) The mean curvature κ_m (averaged along the particle's surface) of nanoparticles as a function of aspect ratios with respect to controlling parameter R. The error bars are estimated by the standard deviation analysis from different batches. As increasing κ_m, the nanoparticle experiences an anisotropic structural transformation. The dotted line indicates that surface curvatures of nanorods can be selectively tuned at a chosen aspect ratio. (c) The projected local surface curvature and AR profiles of each representative nanoparticle at different R. The color bar indicates quantitative curvatures (nm^{-1}) exhibiting both positive and negative values.

a large difference as high as three times. Beyond tuning of the shape and surface facets of nanorods at different aspect ratio by other methods based on binary surfactants [23] our method demonstrated the control of surface curvature even at the same aspect ratio of nanoparticles.

Such a dramatic surface curvature variation with both positive and negative values, therefore, not only has a profound impact on its surface functionalities, but also on their localized surface plasmon properties. Appreciable blueshift of longitudinal plasmonic responses of nanorods are observed as increasing k [Fig. 2(e)]. At the same aspect ratios, the shifting of the surface plasmon resonance of gold nanorods is solely determined by the change of their surface curvatures. Such surface plasmon modifications can be understood by the change of depolarization factors as the shape eccentricity of nanorod varies by its curved surface [33], with well-matched calculation results [Fig. 2(f)]. As such, our unique control of k

could result in an efficient engineered electromagnetic energy distribution along the nanorods. Shown with field depolarization, the plasmonic energy is more confined at highly curved tips [Fig. 2(g)], which could enable a plethora of applications such as Tip or Surface enhanced Raman spectroscopy (TERS, SERS), plasmonic waveguide confinement, biosensors, and near-field single-molecular detections [34–37]. Indeed, the electric-field enhancement (E/E_0) of curved gold nanorod (higher k) is much stronger than the flattened rod with small k at the same aspect ratio. In addition, the measurements on the curvature-dependent SERS based on plasmonic field enhancements directly illustrate the unique application capability of nanoscale curvature in molecule sensing (see Supplemental Material [32], Fig. S5 and Table S1).

Accompanied with surface curvature modification, our supramolecular sculptured synthesis enables further control of anisotropicity and surface deformation of AuNRs

[Fig. 3(a)]. By introducing a small amount of PFOA ($R = 0.027$) as shown, the elongation of AuNRs was observed (average aspect ratio ∼4.0) as compared to $R = 0$ sample [Fig. 2(a). Further increasing R to 0.055 induces even longer nanorods with averaged aspect ratio up to ∼5.1. Moreover, these samples display much improved monodispersity as substantially lower fraction of size and shape impurities, which can be ascribed to the unique surface properties and stiffness of fluorine-rich alkyl chain of PFOA that provide an excellent micellar stability promoting the yield of gold nanorods. It is worth noting that the heads of nanorods become increasingly rounded as raising R, which suggests alterations of k. Very interestingly, instead of elongation, the nanorods are shortened when R is raised to 0.11 and 0.125 [Figs. 2(b) and 2(c), but with identical AR with sample of $R = 0$). The change of aspect ratios is due to the alteration of shape and phase of adsorbed micelles, consistent with previous reports [22,23]. Nanorod shortening continues but exhibits more curved surface ($R = 0.22$). At this higher R ratio, the dispersity in size becomes larger as a result of micellar phase transition due to CTA^+/PFO^- coupling, which broadens ensemble plasmonic responses (Supplemental Material [32], Fig. S6 and Table S2). Further deformation leads to a spherical shape ($R = 0.35$) with average ∼26-nm in diameter. However, the trend of increasing curvature is clearly observed [Fig. 3(b)].

To directly visualize such relationship, the projected AR and the surface curvature profiles were extracted for each representative nanoparticle [Fig. 3(c)]. The correlation between such a structural variation and the mean surface curvature κ_m is exploited as a function of controlling parameter R [Fig. 3(b)]. It can be clearly seen that the increase of κ_m is interdependent with structural change as controlled by R and reflected by the modulation of nanorod aspect ratios. More importantly, the zigzaglike relation as shown could allow one to freely and selectively tailor the surface profiles and hence optical properties of nanoparticles, as demonstrated here, at a chosen aspect ratio (e.g., indicated by projected dotted line).

Fourier transform infrared spectroscopy (FTIR) spectra were employed to confirm the role of coupled hydrocarbon-fluorocarbon supramolecular interactions (Fig. 4). The spectrum of pure PFOA (dotted line) as a comparison shows a strong vibration mode at $1765\,cm^{-1}$ corresponding to the carbonyl group (C = O) free of binding. In contrast, appreciable redshift of this vibrational mode was observed exhibiting lower frequency as increasing R value. This redshift indicates the stretching vibration of carbonyl group is inhibited owing to the synergistic micellization due to strong interactions between PFOA and CTAB [25]. Increasing peak magnitude as raised R implies increasing number of PFOA interacting with CTAB. As a result, the effective positive surface charge from CTA^+ that binds onto the surface gold nanoparticle has been reduced due to the insertion of negative PFO^-, leading to the alteration of surface potentials (Supplemental Material [32], Fig. S7). The vibrational bands of asymmetric and symmetric stretching modes of CH_2 groups at 2925 and $2854\,cm^{-1}$, respectively, are coming from CTAB indicating synergistic coupling effect.

With such evidence of hydrocarbon-fluorocarbon interactions, the phase behaviors of coupled micelles can be understood by the effective critical packing parameter P of
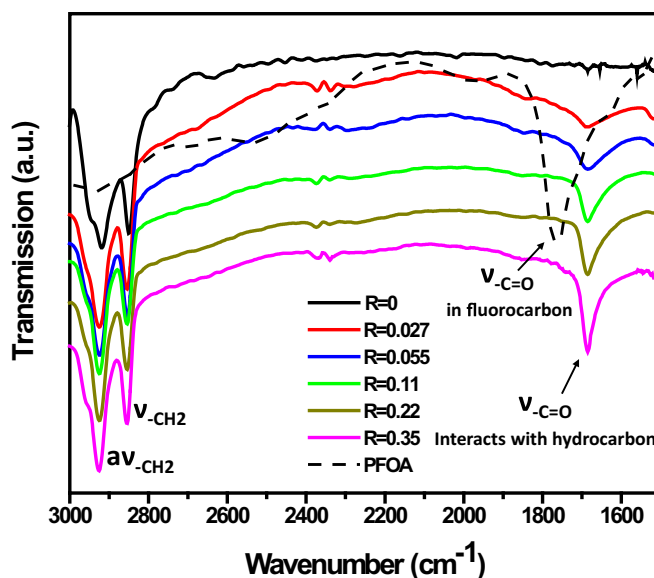

FIG. 4. FTIR reveals synergistic supramolecular coupling. Different colors indicate samples of various R value. The dotted line is the spectrum measured from pure PFOA molecules. Vibration modes of $-C = O$ and $-CH_2$ are marked in the graph. Free-binding carbonyl group (C = O) in pure PFOA experiences an appreciable redshift in wave numbers from 1765 to $1686\,cm^{-1}$ as raising R, indicating strong recognitions and interactions between templating molecules of CTAB and PFOA.

surfactant [38,39], which is given by $P = \frac{V}{a_0 \times l_c}$, where V is the hydrophobic chain volume, a_0 is the mean cross-sectional area of the polar head group, and l_c is the critical length of the hydrocarbon chain. Introducing PFOA increases P by virtue of micelle insertions (increasing V) and reduction of effective a_0 interacting with Au(III) or Au(I) precursor species. The increase of P refines the cylindrical micelles until it reaches its optimal [39,40]. That is why enhanced monodispersity was observed at small R ($R < 0.055$) (Fig. S8). As further introducing PFOA, the phase change of micelle involves cylindrical to bilayered packing with higher value of P which tends to form vesicular structure in aqueous solution [39]. Together with the aid of lipophobic interactions, the micellar packing leads to highly curved gold nanoparticles with a complex level of patchy surface curvatures. When PFOA amount is significantly high, the curved nanostructures are completely closed into vesicular spheres.

IV. CONCLUSION

In summary, we have proposed and demonstrated a supramolecular recognized growth method for one-step sculpturing local surface curvature and anisotropicity of nanoparticle with intriguing plasmonic properties. We have shown that such an important surface geometric factors can be selectively tuned in a broad range of gold nanorods, which is governed by the guest-host chemistry between molecular interplays between hydrocarbon and fluorocarbon supramolecular template. This unique approach may be generalized and ultimately allow for delicate colloidal lithography to nanoscale objects with tailored surface geometric factors, which could

enable platforms for both fundamental study and practical applications in surface chemistry, biology, and optics.

[1] S. Hyde *et al.*, *The Language of Shape: The Role of Curvature in Condensed Matter: Physics, Chemistry and Biology* (Elsevier, Amsterdam, 1996).

[2] B. J. Reynwar *et al.*, Aggregation and vesiculation of membrane proteins by curvature-mediated interactions, Nature (London) **447**, 461 (2007).

[3] H. S. Mandal and H.-B. Kraatz, Effect of the surface curvature on the secondary structure of peptides adsorbed on nanoparticles, J. Am. Chem. Soc. **129**, 6356 (2007).

[4] G.-L. Chai, Z. Hou, D.-J. Shu, T. Ikeda, and K. Terakura, Active sites and mechanisms for oxygen reduction reaction on nitrogen-doped carbon alloy catalysts: Stone-Wales defect and curvature effect, J. Am. Chem. Soc. **136**, 13629 (2014).

[5] A. M. Jackson, J. W. Myerson, and F. Stellacci, Spontaneous assembly of subnanometre-ordered domains in the ligand shell of monolayer-protected nanoparticles, Nat. Mater. **3**, 330 (2004).

[6] H. D. Hill, J. E. Millstone, M. J. Banholzer, and C. A. Mirkin, The role radius of curvature plays in thiolated oligonucleotide loading on gold nanoparticles, ACS Nano **3**, 418 (2009).

[7] B. C. Mei *et al.*, Effects of ligand coordination number and surface curvature on the stability of gold nanoparticles in aqueous solutions, Langmuir **25**, 10604 (2009).

[8] D. Wang *et al.*, How and why nanoparticle's curvature regulates the apparent pK(a) of the coating ligands, J. Am. Chem. Soc. **133**, 2192 (2011).

[9] F. P. Miller, A. F. Vandome, and M. B. John, *Gibbs-Thomson Effect* (VDM Publishing, Riga, 2010).

[10] D. A. Walker, E. K. Leitsch, R. J. Nap, I. Szleifer, and B. A. Grzybowski, Geometric curvature controls the chemical patchiness and self-assembly of nanoparticles, Nat. Nanotechnol. **8**, 676 (2013).

[11] L. Iversen, S. Mathiasen, J. B. Larsen, and D. Stamou, Membrane curvature bends the laws of physics and chemistry, Nat. Chem. Biol. **11**, 822 (2015).

[12] C.-J. Tsou, C.-y. Chu, Y. Hung, and C.-Y. Mou, A broad range fluorescent pH sensor based on hollow mesoporous silica nanoparticles, utilising the surface curvature effect, J. Mater. Chem. B **1**, 5557 (2013).

[13] M. Menon, A. N. Andriotis, and G. E. Froudakis, Curvature dependence of the metal catalyst atom interaction with carbon nanotubes walls, Chem. Phys. Lett. **320**, 425 (2000).

[14] G. Ouyang, C. X. Wang, and G. W. Yang, Surface energy of nanostructural materials with negative curvature and related size effects, Chem. Rev. **109**, 4221 (2009).

[15] S. Chang, Q. Li, X. Xiao, K. Y. Wong, and T. Chen, Enhancement of low energy sunlight harvesting in dye-sensitized solar cells using plasmonic gold nanorods, Energy Environ. Sci. **5**, 9444 (2012).

[16] X. H. Huang, I. H. El-Sayed, W. Qian, and M. A. El-Sayed, Cancer cell imaging and photothermal therapy in the near-infrared region by using gold nanorods, J. Am. Chem. Soc. **128**, 2115 (2006).

[17] S. Yang *et al.*, Feedback-driven self-assembly of symmetry-breaking optical metamaterials in solution, Nat. Nanotechnol. **9**, 1002 (2014).

[18] C. Novo, A. M. Funston, and P. Mulvaney, Direct observation of chemical reactions on single gold nanocrystals using surface plasmon spectroscopy, Nat. Nanotechnol. **3**, 598 (2008).

[19] N. R. Jana, L. Gearheart, and C. J. Murphy, Seed-mediated growth approach for shape-controlled synthesis of spheroidal and rod-like gold nanoparticles using a surfactant template, Adv. Mater. **13**, 1389 (2001).

[20] B. Nikoobakht and M. A. El-Sayed, Preparation and growth mechanism of gold nanorods (NRs) using seed-mediated growth method, Chem. Mater. **15**, 1957 (2003).

[21] J. Perez-Juste, I. Pastoriza-Santos, L. M. Liz-Marzan, and P. Mulvaney, Gold nanorods: Synthesis, characterization and applications, Coord. Chem. Rev. **249**, 1870 (2005).

[22] X. Ye *et al.*, Improved size-tunable synthesis of monodisperse gold nanorods through the use of aromatic additives, ACS Nano **6**, 2804 (2012).

[23] X. Ye, C. Zheng, J. Chen, Y. Gao, and C. B. Murray, Using binary surfactant mixtures to simultaneously improve the dimensional tunability and monodispersity in the seeded growth of gold nanorods, Nano Lett. **13**, 765 (2013).

[24] L. Vigderman and E. R. Zubarev, High-yield synthesis of gold nanorods with longitudinal SPR peak greater than 1200 nm using hydroquinone as a reducing agent, Chem. Mater. **25**, 1450 (2013).

[25] B. Y. Ren, Z. Tong, X. X. Liu, C. Y. Wang, and F. Zeng, Mesomorphous structure and properties of non-equimolar complexes of poly (ethylenimine) and perfluorooctanoic acid, Langmuir **20**, 10737 (2004).

[26] S. Yang *et al.*, On the origin of helical mesostructures, J. Am. Chem. Soc. **128**, 10460 (2006).

[27] M. M. Nejati and M. G. Khaledi, Perfluoro-alcohol-induced complex coacervates of polyelectrolyte-surfactant mixtures: Phase behavior and analysis, Langmuir **31**, 5580 (2015).

[28] A. Kotzev, A. Laschewsky, P. Adriaensens, and J. Gelan, Micellar polymers with hydrocarbon and fluorocarbon hydrophobic chains. A strategy to multicompartment micelles, Macromolecules **35**, 1091 (2002).

[29] T. P. Lodge, A. Rasdal, Z. B. Li, and M. A. Hillmyer, Simultaneous, segregated storage of two agents in a multicompartment micelle, J. Am. Chem. Soc. **127**, 17608 (2005).

[30] L. D. Zarzar *et al.*, Dynamically reconfigurable complex emulsions via tunable interfacial tensions, Nature (London) **518**, 520 (2015).

[31] M. Grzelczak *et al.*, Influence of iodide ions on the growth of gold nanorods: Tuning tip curvature and surface plasmon resonance, Adv, Funct. Mater. **18**, 3780 (2008).

[32] See Supplemental Material at http://link.aps.org/supplemental/10.1103/PhysRevMaterials.3.116002 for detailed growth method, surface curvature analysis, curvature-dependent SERS, and additional molecular and nanoparticle characterizations.

[33] S. W. Prescott and P. Mulvaney, Gold nanorod extinction spectra, J. Appl. Phys. **99**, 123504 (2006).

[34] K. A. Willets and R. P. Van Duyne, Localized surface plasmon resonance spectroscopy and sensing, Annu. Rev. Phys. Chem. **58**, 267 (2007).

[35] P. Zijlstra, P. M. R. Paulo, and M. Orrit, Optical detection of single non-absorbing molecules using the surface plasmon resonance of a gold nanorod, Nat. Nanotechnol. **7**, 379 (2012).

[36] D. Lee and S. Yoon, Effect of nanogap curvature on SERS: A finite-difference time-domain study, J. Phys. Chem. C **120**, 20642 (2016).

[37] C. Sonnichsen, B. M. Reinhard, J. Liphardt, and A. P. Alivisatos, A molecular ruler based on plasmon coupling of single gold and silver nanoparticles, Nat. Biotechnol. **23**, 741 (2005).

[38] J. N Israelachvili, *Intermolecular and Surface Forces*, 3rd ed. (Academic, London, 2011).

[39] M. Antonietti and S Forster, Vesicles and liposomes: A self-assembly principle beyond lipids, Adv. Mater. **15**, 1323 (2003).

[40] R. M. Pallares, X. Su, S. H. Lim, and N. T. K. Thanh, Fine-tuning of gold nanorod dimensions and plasmonic properties using the Hofmeister effects, J. Mater. Chem. C **4**, 53 (2016).